IMPROVED DEPTH-PHASE DETECTION AT REGIONAL DISTANCES

Delaine Reiter and Anastasia Stroujkova

Weston Geophysical Corporation

Sponsored by National Nuclear Security Administration
Office of Nonproliferation Research and Engineering
Office of Defense Nuclear Nonproliferation

Contract No. DE-FG02-03ER83820

ABSTRACT

The accurate estimation of the depth of small, regionally recorded events continues to be an important and difficult monitoring research problem. In previous studies we have focused on the extraction of depth phases from body waves using cepstral techniques, with greater success at teleseismic rather than regional distances. To further enhance the accuracy of regional focal depth estimation, other waveform characteristics that are sensitive to depth must be exploited. The primary goal of our current research project is to develop a synergistic tool that combines different methodologies to estimate the depth of regional seismic events. The three methods we are incorporating include: a) improved depth-phase detection in the complex *Pn* coda of regional seismograms; b) sparse-network locations with Monte Carlo confidence regions on focal depth; and c) surface-wave inversions for depth and focal mechanism. We have chosen to apply these three methods rather than full-waveform modeling of the regional seismograms, primarily because the observables used in these methods are significantly easier to measure and model.

As part of our research project we have focused on understanding the propagation characteristics of regional depth phases and developing robust methods to routinely detect them. To accomplish this goal, we have computed synthetic seismograms for regional events observed at regional and teleseismic arrays in Asia. For each of these events, we varied the input velocity model, focal mechanism, and source depth. In addition to waveform modeling, we have applied array-processing techniques to derive accurate estimates of phase velocities, azimuth, and coherence as a function of time in the *Pn* wavetrain. These studies indicate that cepstral depth-phase detection results should be accompanied by estimates of the focal mechanism, phase velocities and back azimuths to help eliminate false detections.

We have also continued research on improvements to the cepstral processing technique, known as the Cepstral F-Statistic Method (CFSM) that we have employed in the past (Bonner et al., 2002). The application of cepstral 'liftering' (or filtering in the log spectrum domain) is a topic of active research, as is robust denoising of the array waveforms prior to application of the cepstral technique. One denoising method that is showing some promise is semblance filtering of the array waveforms. This method measures phase coherence that can then be used to filter or 'weight' the array element data.

Improved regional depth-phase detections combined with depth estimates measured from other waveform observables will provide the Air Force Technical Applications Center (AFTAC) with increased confidence that an event is either deep enough to be ruled out as a nuclear explosion or shallow enough to require further analysis using regional discriminants such as M_s:m_b or *Lg/P* ratios. Our goal is to develop an analysis tool that can be used on a special-event basis to improve the US government's ability to correctly classify events as either man-made explosions or naturally-occurring earthquakes.

OBJECTIVES

The primary goal of our project is the development of a synergistic tool that combines three different technologies to estimate the depth of regional seismic events. These methods include 1) improved depth phase detection in the complex *Pn* coda of regional seismograms; 2) sparse-network hypocenter locations with associated Monte-Carlo confidence regions; and 3) surface-wave spectral amplitude inversions for depth and moment magnitude. In the first year of the project we have focused on the first of these methods: improved depth-phase detection. To accomplish this we have conducted multiple modeling exercises using standard 1-D and 2-D modeling codes to examine the effects that different focal mechanisms and velocity structures have on the frequency, relative amplitudes, and travel times of regional depth phases. We also continue to test and add further capabilities to the Cepstral F-Statistic Method (CFSM) (Bonner et al., 2002), which is designed to determine the delay time between *pPn* and/or *sPn* and the primary *Pn* arrival. Finally, we are investigating innovative filtering techniques to enhance regional depth phases in the *Pn* coda, and we report on a promising method that utilizes semblance-based weighting on array element data.

RESEARCH ACCOMPLISHED

Synthetic Studies of Regional Depth-Phase Characteristics

We conducted a series of synthetic modeling experiments using a variety of focal mechanisms and velocity structures to better understand the amplitudes and travel times of *Pn* and its associated depth phases, *pPn* and *sPn*. Our specific purpose in these exercises was to determine if the CFSM, which relies on observable energy in the depth phases to robustly estimate the depth-phase delay time (*pPn-Pn* or *sPn-Pn*), will be successful at regional distances. In this paper we show examples from two events observed at the Kazakhstan arrays, MKAR (Makanchi) and KKAR (Karatau), noting that we are also studying other events at several arrays in central and southeastern Asia. Figure 1a) shows the event, along with the published Harvard Central Moment Tensor (CMT) solution and the positions of the MKAR and KKAR arrays.

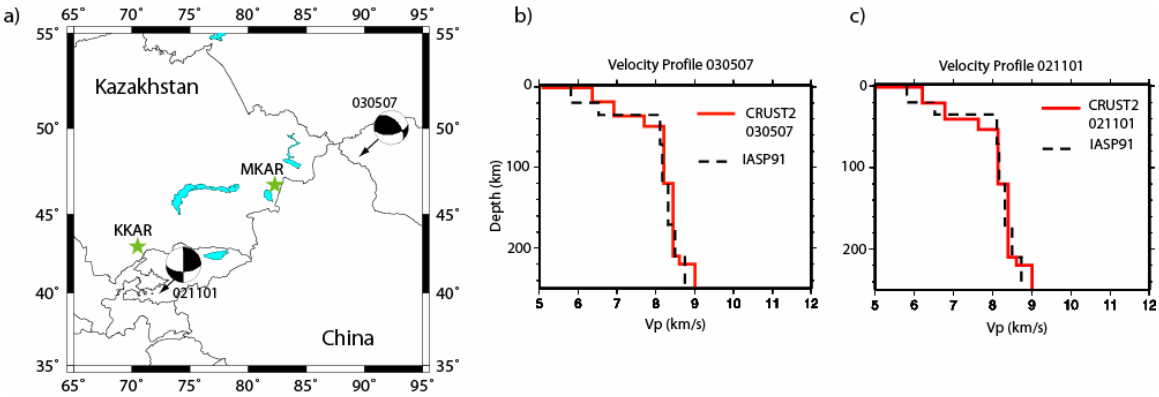

Figure 1. Locations and models for events examined in this paper. a) Event locations and published Harvard CMT solutions for events in Mongolia (05/07/03) and Kyrghystan (11/01/02); b) regional 1-D velocity profile for Event 030507 interpolated from the CRUST2.0 velocity model (Bassin et al., 2002); c) same as b) but for Event 021101. The IASPEI91 average global 1-D model is shown for comparison in both b) and c).

To generate the synthetics, we used the wavenumber integration code from the Computer Programs in Seismology (Herrmann, 2002; CPIS), which requires a 1-D layered velocity structure for input. We selected an appropriate regional profile from the CRUST2.0 velocity model (Bassin et al., 2002), merging the two sediment layers together and appending the regionalized upper mantle (RUM) model for the upper mantle structure (Gudmundsson and Sambridge, 1998). The V_p structures used in the modeling are shown in Figure 1b) and 1c), along with their comparison to the IASPEI91 global model (Kennett and Engdahl, 1991).

We calculated waveform synthetics, holding the focal mechanism and velocity structure constant and varying the event depth. For example, in Figure 2 we show the synthetic calculations for event depths Z=2, 6, 10, 14, 18, 22 and 30 km at MKAR for Event 030507. The depth phases are clearly seen in the synthetics, with *sPn* having significantly larger amplitude. This amplitude increase is not seen in the data (lower panel) and appears to be a quirk of the wavenumber integration method. Overall, our modeling for this and other events indicates that differences in focal depth only slightly change the relative amplitudes of *Pn*, *pPn* and *sPn* (the first three significant arrivals in the synthetics).

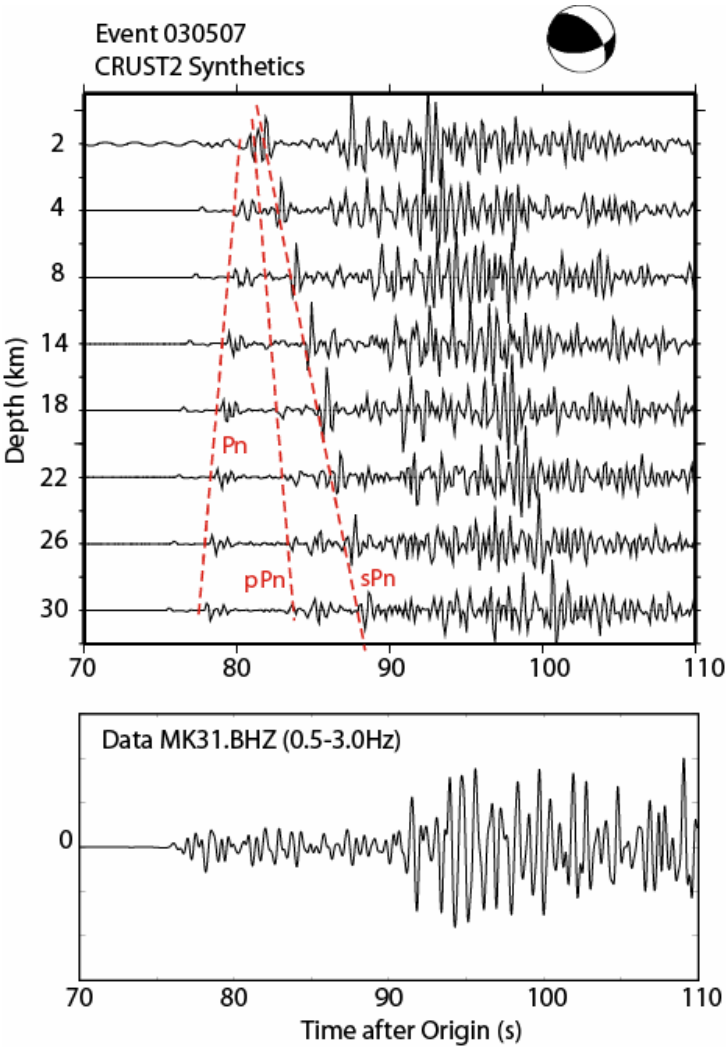

Figure 2. Top: Synthetic calculations for Event 030507, using the Harvard CMT focal mechanism, the velocity model shown in Figure 1c) and varying the depth. The *Pn* arrival, its depth phases, and *Pg* are marked by dotted lines. Bottom: The vertical component of the broadband instrument installed at the MKAR array.

Next, we calculated synthetics in which we held the event depth constant and varied the focal mechanism. We chose an arbitrary depth of 6 km, since the synthetics show similar characteristics for all depths as a function of focal mechanism. Our results indicate that differences in focal mechanism play the dominant role in the amplitude relationships and frequency content of *Pn* and its depth phases. For example, in Figure 3a) we present the results for strike-slip mechanisms. For this type of mechanism, the orientation of the nodal planes changes only the absolute amplitudes, which preserves the relative amplitudes between *Pn*, *pPn* and *sPn*. However, the amplitudes of the depth phases are much more sensitive to the dip-slip

component of the mechanism, as shown in Figure 3b; in fact, for many focal mechanisms there is no appreciable depth-phase energy. The results of these modeling exercises confirmed that an estimate of the focal mechanism must be part of a regional depth-phase detection methodology, since it will provide an indication of whether the depth phases will have appreciable amplitudes in the *Pn* coda.

Finally, we have observed that mid-crustal refractions (e.g., *Pb*) can interfere with the depth phases, particularly at shorter distances ($\Delta < 3.5$-4°). Some areas we studied in central Asia do exhibit this type of arrival, which means that the presence of such phases should be identified through array processing to eliminate them from contention as regional depth phases. In fact, the application of cepstral processing for depth phase delays at distances shorter than approximately 4° is difficult, due to the interference of upper and mid-crustal secondary phases at nearly the identical travel times as the depth phases.

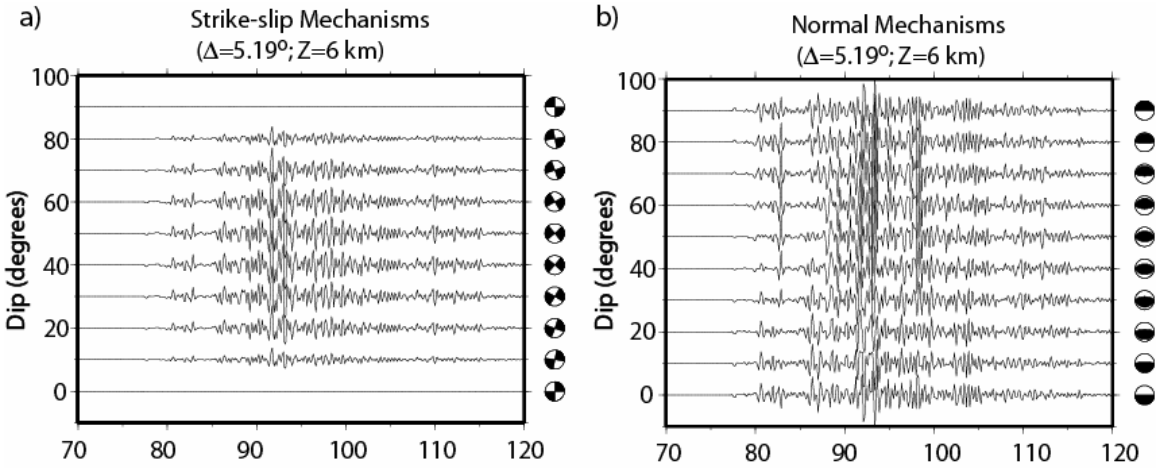

Figure 3. Synthetic waveforms demonstrating the effects that focal mechanisms have on the *Pn* arrival, its depth phases, and later coda arrivals. a) Strike-slip mechanisms for an earthquake at 6-km depth, at the same distance as MKAR from Event 030507 (Δ=5.19°); b) normal mechanisms for the same distance and focal depth.

The Cepstral F-Statistic Method: Liftering to Improve Delay Estimates

In previous work (Bonner et al., 2002), we presented a focal-depth estimation method using a cepstral F statistic (the CFSM) that provides a statistical estimate of the significance of peaks in a stacked cepstrum. We calculate the power cepstrum, as defined by Bogert et al. (1963), as the Fourier transform of the log spectrum of a windowed time signal. The classic paper by Bogert et al. (1963) also introduced the concept of liftering as part of cepstrum computation. Liftering is literally linear filtering of the log spectrum, and its purpose is to emphasize the periodic component of the log spectrum (rather than the spectral envelope), thereby enhancing the detectability of echoes. Researchers in speech analysis noted that by applying a low-pass lifter to the cepstrum, they could extract low-quefrency components that were indicative of the resonance structure of the vocal tract (Noll, 1967). The application of liftering to seismic data, however, is more problematic (Childers et al., 1977), because of the inherent noisiness and limited bandwidth in the data. We are investigating the benefits and limitations of liftering in the log spectra of regional seismic array data, specifically to determine the potential improvement to focal depth estimates using the CFSM.

Liftering is useful in the CFSM in two ways; first, we can use it to eliminate low-quefrency values (i.e., low delay times). In Figure 4, we illustrate the use of liftering in the CFSM. Figure 4 is a typical display of the output from the CFSM; in the top panel, we show the beam cepstrum (summed cepstra across the array) and the total cepstrum (cepstrum of the mean array log spectrum). In the lower panels, we show the calculated F statistic along with the 95% confidence line (see Bonner et al. (2002) for more details on the CFSM). All peaks above the confidence line can be considered 'significant'; however, not all of them have any physical meaning. We always look for confirmation of peaks in the beam and total cepstrum to accompany peaks in the F statistic. As we illustrate in Figure 4, without the use of liftering (Figure 4a), it is

difficult to interpret low-quefrency cepstral values, since noise from the early cepstrum dominates the F-statistic delay-time estimate. In the past, we restricted analysis of the final cepstral estimates to quefrency values above 2.5 seconds, which meant that we could only evaluate event depths greater than approximately 15 km. With the use of liftering (Figure 4b) we can specify the precise number of seconds to eliminate in the final cepstral estimate. Currently, we lifter out the first .9 seconds of the cepstrum in the CFSM; however, we continue to test to determine the most appropriate value.

Cepstral liftering also allows us to set the length of window to retain in the final cepstral calculation, so that we can define the exact delay-time window that we are most interested in. This allows the user to input a much longer analysis window of raw data from the seismogram, which presumably contains the reflected phases of interest and their later-arriving multiples. Then, through liftering, the final log spectrum has high-frequency 'chatter' eliminated prior to the final FFT. We currently limit the output delay-time (quefrency) window to 13 seconds, theorizing that interesting depth phase reflections for most events at regional distances will occur within 13 seconds of the *Pn* (first) arrival. The 13-second limit is equivalent to restricting the search to depth-phase delays from events up to approximately 14° away in epicentral distance with depths up to 40 km (using theIASPEI91 model).

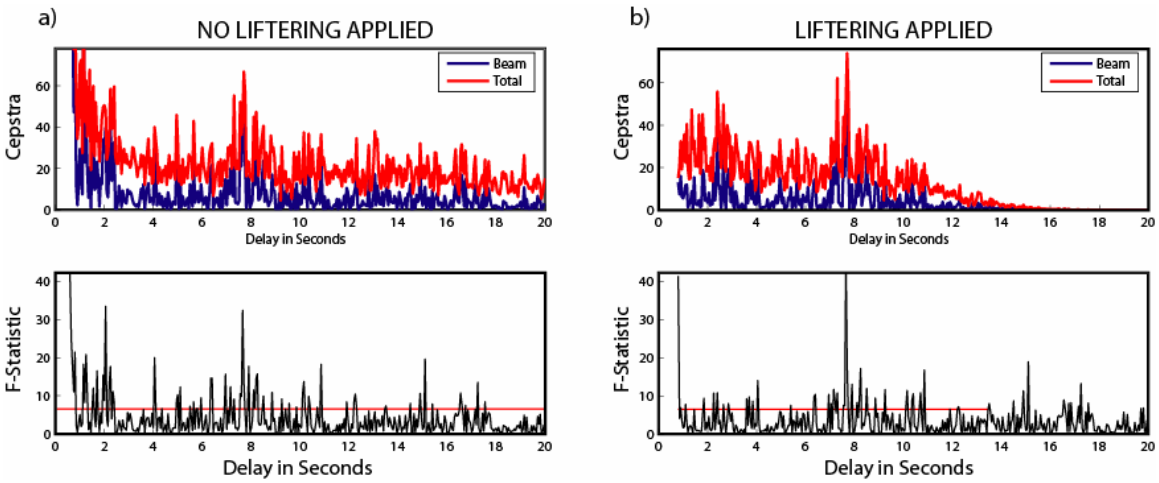

Figure 4. a) An example of an application of the CFSM to the MKAR data for Event 021101 in which no liftering has been applied. b) The same data as in a), except liftering has been performed in the log spectrum domain between the equivalent of .9 and 13 seconds. Note the diminished amplitudes in the low delay times (1-6 seconds), which is due to the removal of high-frequency noise in the log spectrum domain. When we incorporate liftering, we also do not interpret cepstral peaks above 13 seconds.

Improved Filtering and Enhancement of Regional Depth Phases

During the first year of the project, we investigated methods that could be used to enhance or isolate the depth phases in regional data. One method that is showing promise involves semblance weighting of the first arrival and its coda. We judge a filtering method's usefulness by comparing the performance of the CFSM before and after a particular filtering technique is applied to the data.

Semblance Weighting. A convenient measure of coherence across a seismic array is provided by semblance (Taner and Koehler, 1969). Semblance weighting is commonly used in exploration geophysics to enhance small but coherent arrivals in reflection data. The semblance between L traces of an array for i^{th} time index is defined as

$$S_i = \frac{\sum_{w=-W/2}^{W/2}\left[\sum_{j=1}^{L} y_j(i+w)\right]^2}{N\sum_{w=-W/2}^{W/2}\sum_{j=1}^{L}\left[y_j(i+w)\right]^2}, \quad (1)$$

where L is the number of traces, j is the trace for which the semblance weighting is applied, and $y_j(i)$ is the sample of the seismic trace. The stacking is performed over a time gate W, which for stability reasons should be larger than the period of the phase being filtered. The semblance is always positive and ranges between 0 and 1. It is close to unity for coherent events and approaches *1/N* otherwise.

If the array is beamed along linear distance-arrival time (i.e., $X - T$) trajectories, defined by horizontal ray parameters, then the semblance can be estimated along the same trajectories. In this case, an appropriate time shift must be added to the sample number i. Semblance weighting of the seismic traces can then be performed along these trajectories:

$$y_j^s(i) = S_i y_j(i) \quad (2)$$

In Figure 4 we show examples of semblance weighting applied to data from the MKAR and KKAR arrays for the 021101 Kyrghystan event. The upper panels of Figure 4a and 4b show the semblance values along the beamed seismogram as a function of back azimuth with a color scale ranging from 0.1 (magenta) to 1 (red). The maximum semblance value indicates an apparent azimuth of arrival for each arriving phase. A dashed horizontal line shows the positions of the International Seismological Centre (ISC) bulletin's back azimuth for comparison. In the bottom panels of Figures 4, we show the array beams before (black lines) and after (red lines) semblance weighting. The semblance weighting was performed along the $X - T$ trajectories using the direction of the apparent azimuth of the first arrival and the slowness derived from V_p (as shown in the figures). The predominant effect of the semblance weighting procedure for this example is the reduction of amplitudes for incoherent arrivals.

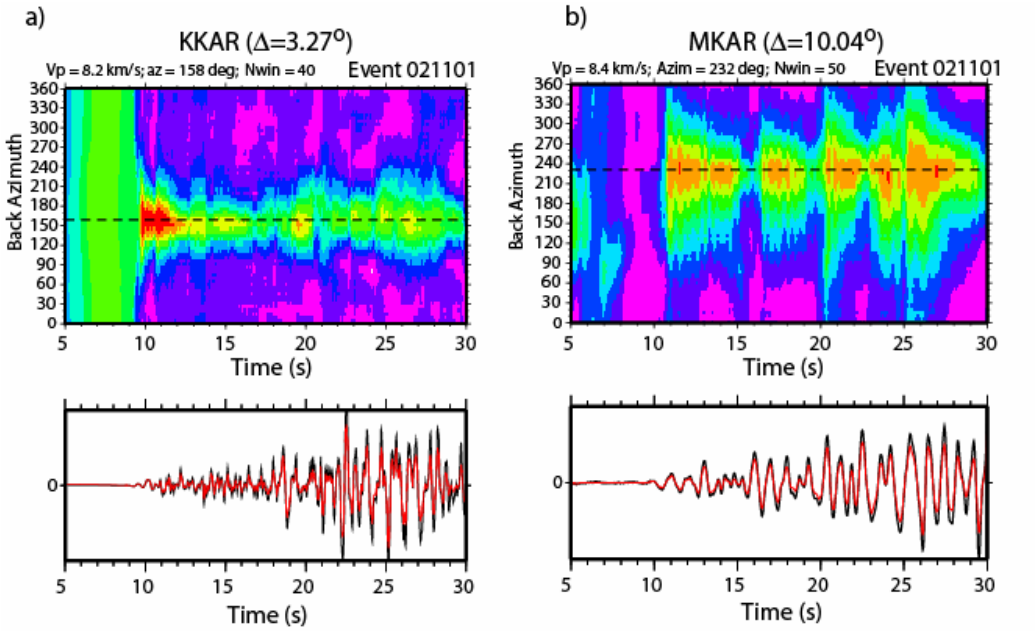

Figure 5. a) Semblance processing for Event 021101 recorded at KKAR. Top panel shows semblance as a function of back azimuth, assuming V_p = 8.2 km/s. b) Same for MKAR, with V_p = 8.2 km/s.

Another example of semblance weighting is shown in Figure 5 for Event 030507. In this case there is a considerable difference (about 20º) between the published and inferred back azimuths for the *Pn* arrival. This may be explained by either significant inhomogeneity in the crust or changes in Moho depth between the earthquake and the array.

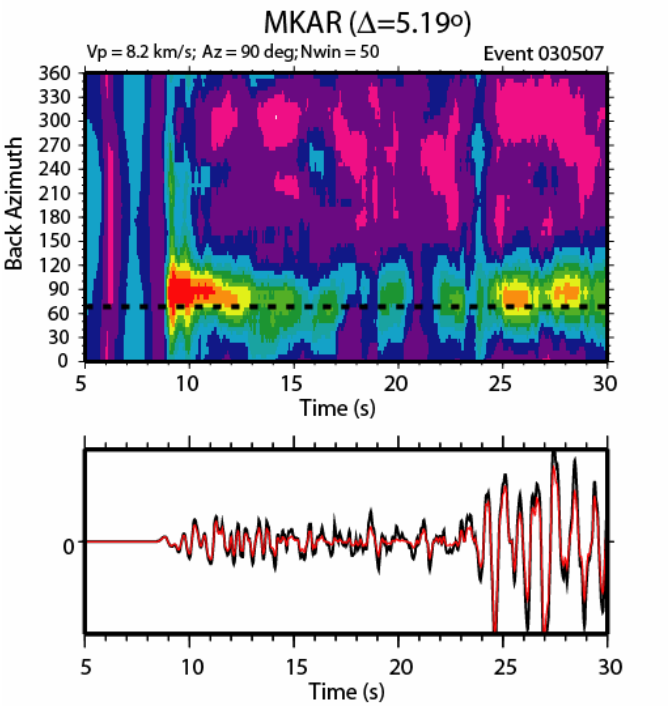

Figure 6. Semblance processing for Event 030507, assuming V_p = 8.2 km/s. The azimuth estimated by semblance for the MKAR array is nearly 20° greater than the one published by the ISC.

Application of Semblance Weighting to the CFSM. We are currently testing the effectiveness of the semblance weighting method as a pre-filtering method for the CFSM. For example, we show the results of applying the CFSM to the MKAR data from Event 021101 in Figure 7. Figure 7a) shows the unfiltered individual array waveforms in the top panel (we note that element MK09 was not available for this event) and the cepstral analysis results in the bottom two panels. Figure 7b) shows the same results for the semblance-weighted array data. It is somewhat difficult to see significant changes between the unfiltered and semblance-weighted array waveform data, but the changes in the cepstral quantities are significant. In particular, the unfiltered data has significantly larger peaks in the beam and total cepstrum at delay times between 2-6 seconds than do the results the semblance-weighted data. Also, the peak at approximately 7.5 seconds in the CFSM results is more pronounced with the semblance-weighted data. We have observed the low delay-time effects for many applications of the CFSM using unfiltered and semblance-weighted data. Another example of this type of behavior, albeit not as pronounced is shown in Figure 8, in which we performed the same analysis for Event 021101 with the KKAR data.

The results from the cepstral analyses of the KKAR and MKAR data for Event 021101 are quite different from each other. KKAR is at a distance of 3.27° for this event, and travel-time predictions using the model in Figure 1c) indicate that the secondary crustal phases *Pb* and *PnPn* should arrive very close to the *Pn* depth phases (*pPn* and *sPn*). The KKAR cepstral analysis reflects this muddied succession of arrivals, with no isolated and prominent peaks in the beam or total cepstrum, or in the F-statistic. On the other hand, the MKAR cepstral analysis reveals a clear peak (or possibly double peak) near 7.5-8.0 seconds delay time. At a focal depth of 15 km, this peak corresponds to the delay times for the *sPn* and *PnPn* phases, which arrive at nearly the same time following *Pn* at this distance (10.04°). The ISC bulletin lists focal depths from various agencies for this event that range from 10-33km, and teleseismic depth phase constraints fixed the

depth to be 10.4 ± 1.88 km. Our results are within range of that depth, given the limited regional array data we analyzed for the event. Finally, array analysis (not shown here) of the MKAR and KKAR data using a robust cross-correlation technique (Tibuleac and Herrin, 1997) confirms our cepstral analysis.

CONCLUSIONS AND RECOMMENDATIONS

The first year of this project was focused on improving the regional capabilities of the CFSM. Several conclusions can be drawn from this work: First, the proper application of the CSFM should be accompanied by an estimate of the focal mechanism of the event (even a preliminary one) and an array analysis of phase slowness, travel time and azimuth. Second, the application of liftering in the log spectrum prior to final calculation of the cepstrum can reveal hidden details in the quefrency (delay time) domain that are not apparent. In the next year we will attempt to confirm the usefulness of liftering for regional seismic data. Finally, pre-filtering array data using a semblance-weighting technique appears to reduce noise in the CSFM results.

During the next year, we will complete the development and testing of a multi-objective optimization technique to estimate regional focal depths. This technique will incorporate depth estimates made from regional surface waves, depth-phase detections in the Pn coda and possibly sparse-network hypocenter locations. We believe that the synthesis of results from multiple data types will be required for the successful estimation of depth at regional distances.

ACKNOWLEDGEMENTS

We are grateful to Drs. Jessie Bonner and Ileana Tibuleac for advice and discussion related to many of the topics discussed in this paper. All maps were produced using the Generic Mapping Tools (GMT) data processing and display package (Wessell and Smith, 1991; 1995).

REFERENCES

Bassin, C., G. Laske and G. Masters (2000), The Current Limits of Resolution for Surface Wave Tomography in North America, *EOS Trans AGU* 81, F897.

Bogert, B. P., M. J. R Healy, and J. W. Tukey (1963), The quefrency analysis of time series for echoes: Cepstrum, pseudo-autocovariance, cross-cepstrum, and saphe cracking, in *Time Series Analysis*, M. Rosenblatt, Ed., Ch. 15: 209–243.

Bonner, J. L., D. T. Reiter, and R. H. Shumway (2002), Application of a cepstral F-statistic for improved depth estimation, *Bull. Seism. Soc. Am* 92, 1675–1693.

Childers, D. G., D. P. Skinner, and R. C. Kemerait (1977), The cepstrum: a guide to processing, *Proceedings of the IEEE* 65: 1428–1443.

Gudmundsson, O. and Sambridge, M. (1998), A regionalized upper mantle (RUM) seismic model, *J. Geophys. Res.* 103: 7121–7136.

Herrmann, R. B. (2002), *Computer Programs in Seismology* Version 3.20, St. Louis University.

Kennett, B. L. N., and E. R. Engdahl (1991), Travel times for global earthquake location and phase identification, *Geophys. J. Int*. 105: 429–465.

Noll, A.M. (1967), Cepstrum pitch determination, *J. Acoust. Soc. Am*. 41: 293–309.

Taner, M. T., and F. Koehler (1969), Velocity spectra – digital derivation and applications of velocity functions, *Geophysics* 34: 859–881.

Tibuleac, I.M., and E. T. Herrin (1997), Calibration studies at TXAR, *Seism. Res. Lett.* 68: 353–365.

Wessel, P., and W. H. F. Smith (1991). Free software helps map and display data, *Eos Trans. AGU* **72**: 441, 445–446.

Wessel, P., and W. H. F. Smith (1995). New version of the Generic Mapping Tools released, *Eos Trans. AGU* 76: 329.

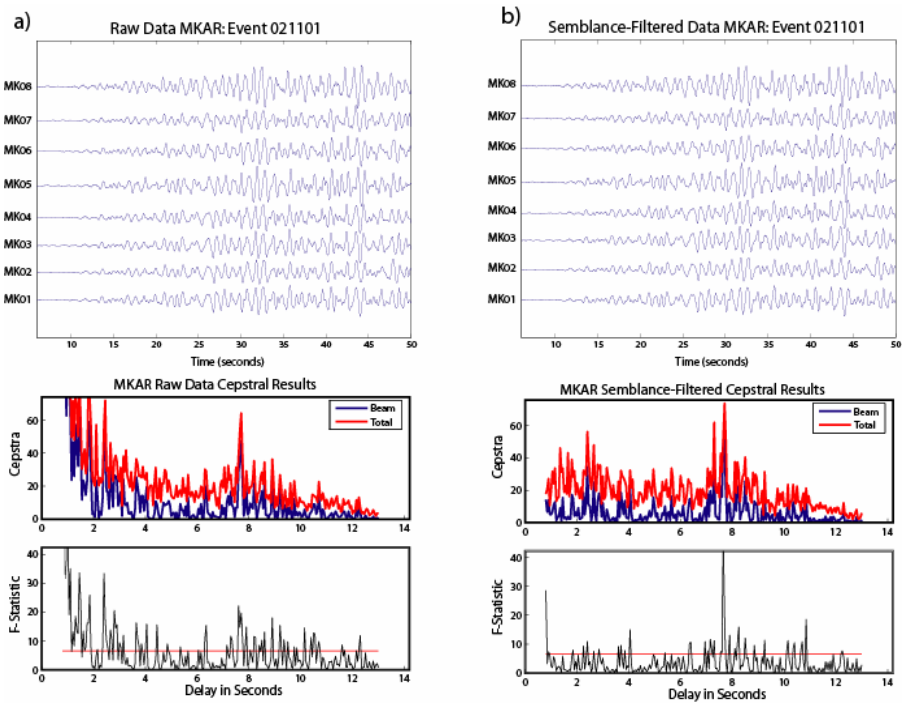

Figure 7. Event 021101: Comparison of the CFSM for unfiltered and semblance-weighted MKAR data. a) Top panel shows the unfiltered array data, middle and bottom panels show the results from the CFSM; b) same as a) but with semblance-weighted data input to the CFSM.

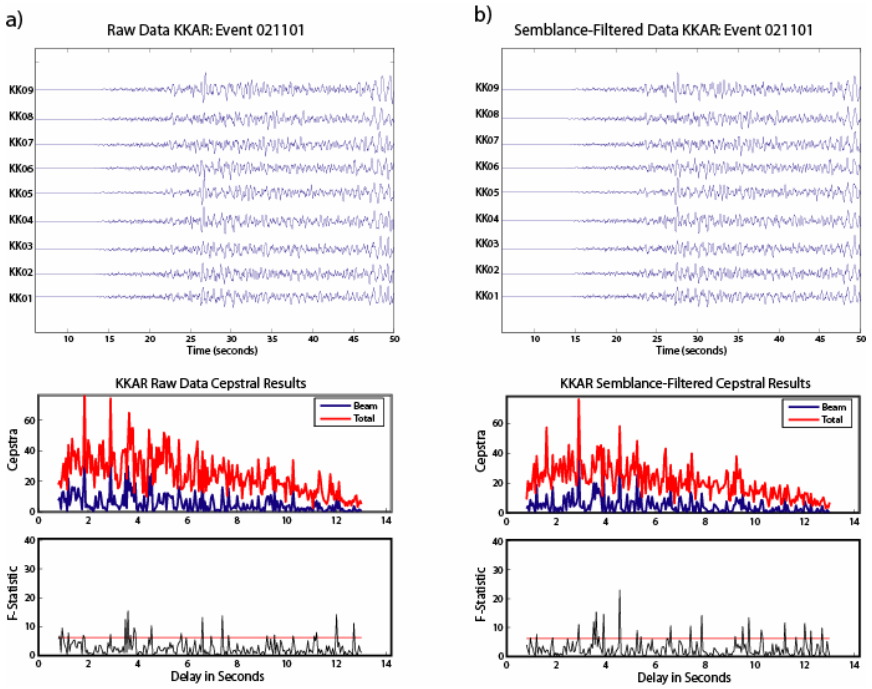

Figure 8. Event 021101: Comparison of the CFSM for unfiltered and semblance-weighted KKAR data. a) The top panel shows the unfiltered array waveforms, and the middle and bottom panels provide results from the CFSM; b) same as in a) but with semblance-weighted data used as input to the CFSM.